ELSEVIER

Cardiovascular Pathology 10 (2001) 69–82

CARDIOVASCULAR PATHOLOGY

Raman microspectroscopy of human coronary atherosclerosis: Biochemical assessment of cellular and extracellular morphologic structures in situ

Hendrik P. Buschman[a,b,*], Geurt Deinum[b], Jason T. Motz[b], Maryann Fitzmaurice[c], John R. Kramer[d], Arnoud van der Laarse[a], Albert V. Bruschke[a], Michael S. Feld[b]

[a]*Leiden University Medical Center, Leiden, The Netherlands*
[b]*Massachusetts Institute of Technology, Cambridge, MA, USA*
[c]*University Hospitals of Cleveland and Case Western Reserve University, Cleveland, OH, USA*
[d]*The Cleveland Clinic Foundation, Cleveland, OH, USA*

Received 17 May 2000; received in revised form 28 February 2001; accepted 12 March 2001

Abstract

Background: We have previously shown that Raman spectroscopy can be used for chemical analysis of intact human coronary artery atherosclerotic lesions ex vivo without tissue homogenization or extraction. Here, we report the chemical analysis of individual cellular and extracellular components of atherosclerotic lesions in different stages of disease progression in situ using Raman microspectroscopy. *Methods:* Thirty-five coronary artery samples were taken from 16 explanted transplant recipient hearts, and thin sections were prepared. Using a high-resolution confocal Raman microspectrometer system with an 830-nm laser light, high signal-to-noise Raman spectra were obtained from the following morphologic structures: internal and external elastic lamina, collagen fibers, fat, foam cells, smooth muscle cells, necrotic core, β-carotene, cholesterol crystals, and calcium mineralizations. Their Raman spectra were modeled by using a linear combination of basis Raman spectra from the major biochemicals present in arterial tissue, including collagen, elastin, actin, myosin, tropomyosin, cholesterol monohydrate, cholesterol linoleate, phosphatidyl choline, triolein, calcium hydroxyapatite, calcium carbonate, and β-carotene. *Results:* The results show that the various morphologic structures have characteristic Raman spectra, which vary little from structure to structure and from artery to artery. The biochemical model described the spectrum of each morphologic structure quite well, indicating that the most essential biochemical components were included in the model. Furthermore, the biochemical composition of each structure, indicated by the fit contributions of the biochemical basis spectra of the morphologic structure spectrum, was very consistent. *Conclusion:* The Raman spectra of various morphologic structures in normal and atherosclerotic coronary artery may be used as basis spectra in a linear combination model to analyze the morphologic composition of atherosclerotic coronary artery lesions.

Keywords: Atherosclerosis; Coronary artery disease; Biochemistry; Morphology; Raman spectroscopy

1. Introduction

Raman spectroscopy has great potential for biochemical analysis of tissue on both the macroscopic and microscopic scale. One of the great advantages of this technique is its ability to provide information about the concentration, structure, and interaction of biochemical molecules in their microenvironments within intact cells and tissues (i.e. in situ), nondestructively, without homogenization, extraction, or the use of dyes, labels, or other contrast-enhancing agents. In addition, Raman spectroscopy can be performed in vivo using optical fiber technology.

Raman spectroscopy has been used previously in studies of isolated or cultured cells, for such purposes as identification of intracellular cholesterol crystals in cultured endothelial cells [1], DNA identification in metaphase chromosomes in isolated human salivary gland cells [2], and DNA and phospholipid identification in periph-

* Corresponding author. Present address: Twente Institute for Neuromodulation Medisch Spectrum Twente, PO Box 50000, 7500 KA Enschede, The Netherlands. Tel.: +31-53-4872840/+31-53-4872802; fax: +31-53-4873100.

E-mail address: r.buschman@rrd.nl (H.P. Buschman).

1054-8807/01/$ – see front matter
PII: S1054-8807(01)00064-3

eral blood lymphocytes [3]. Raman spectroscopy has also been used for the identification and pathophysiological characterization of normal and diseased tissues, including the lens of the human eye [4]. The number of new diagnostic applications is growing rapidly. Recent applications in cancer research include studies of benign and malignant skin lesions and solid tumors in the colon, lung, and liver [5–9].

To date, the most advanced applications of Raman tissue spectroscopy are in atherosclerotic vascular disease. Current atherosclerosis research focuses on unstable plaques, with a thin fibrous cap overlying a large pool of necrotic lipid material (the atheroma core) comprised largely of cholesterol [10–12]. Recent studies have shown that chemical composition and morphology, rather than anatomy (degree of stenosis), determine atherosclerotic plaque stability and predict disease progression and the risk of life-threatening complications such as thrombosis and acute plaque hemorrhage [13–21]. For example, chemical constituents such as cholesterol esters may soften the plaque, whereas crystalline-free cholesterol may have the opposite effect [18,19]. The presence of morphologic constituents such as foam cells and other inflammatory cells may also play a role in plaque instability [20,21]. Raman spectroscopy is ideally suited to analyze these tissue factors, both in vitro and in vivo.

In previous studies, we have used Raman spectroscopy for quantitative biochemical analysis of intact (nonhomogenized or extracted) aorta and coronary artery tissue in vitro [22–31]. In these macroscopic studies, the biochemical analysis was performed by modeling the Raman tissue spectra using a simple linear combination of basis Raman spectra from the major biochemicals present in arterial tissue. Algorithms were then devised to diagnostically classify these tissues as either nonatherosclerotic or calcified or noncalcified atheromatous plaque, based on their biochemical composition [31]. These studies have clearly demonstrated that in situ Raman spectroscopic analysis can be used for the diagnosis of atherosclerosis in intact vascular tissue in vitro. With the use of optical fiber probes, this type of biochemical analysis can even be used to assess atherosclerosis in vivo.

However, morphologic factors may be as important as biochemical composition in determining plaque stability and progression. The present study investigates the feasibility of morphology-based diagnosis of atherosclerotic lesions in arterial tissue using Raman spectroscopy. To that end, in situ Raman spectra of individual cellular and extracellular components of normal and atherosclerotic human coronary artery tissue were obtained in vitro using confocal Raman microspectroscopy. The biochemical composition of these microscopic morphologic structures were then determined by modeling their Raman spectra using a linear combination of basis Raman spectra of biochemicals in a similar way as used previously for intact tissue. In follow-up studies [32], the Raman spectra of these morphologic structures will be used, in turn, as basis spectra in a linear combination model to perform a relative comparison of the morphologic composition of atherosclerotic lesions. Analogous to the macroscopic Raman spectroscopy biochemical analyses, these macroscopic Raman spectroscopy morphologic analyses could ultimately be used in a diagnostic algorithm to assess atherosclerotic plaque stability and disease progression in vivo [33,34].

2. Materials and methods

2.1. Tissue preparation

Human coronary artery samples ($n = 35$), exhibiting varying stages of atherosclerosis, were obtained from explanted recipient hearts ($n = 16$) within 1 h of heart transplantation. Immediately after dissection from the explanted hearts, the artery samples were rinsed with neutral buffered saline, snap frozen in liquid nitrogen, and stored at $-85°C$.

Frozen coronary artery samples were mounted on a cryostate chuck with Histoprep (Fisher Diagnostics, Orangeburg, NY). Thin transverse tissue sections (6–8 μm) for light microscopy and Raman microspectroscopy were cut using a cryostat/microtome (International Equipment, Needham Heights, MA). Four sections of each sample were mounted on glass microscope slides and stained with hematoxylin and eosin. Serial unstained sections were then mounted on BaF_2 or MgF_2 flats (International Scientific Products, Tarrytown, NY, and Spectra-Tech., Stamford, CT), kept moist with phosphate buffered saline (pH 7.4), and transferred to the microscope stage for spectroscopic experiments performed at room temperature. No coverslip was used for spectroscopic measurements. If spectra were collected from a large number of morphologic structures, each section was replaced by a freshly cut section after approximately 2 h to avoid biochemical changes in the tissue as a result of enzymatic degradation. No significant changes were seen in the Raman spectra within this 2-h period of study. The morphologic structures examined were in normal arteries: collagen fibers in the various layers of the arterial wall, internal and external elastic laminae, medial smooth muscle cells, and adventitial fat cells, and in intimal atherosclerotic lesions: collagen fibers in the fibrous cap, foam cells, necrotic core, cholesterol crystals, β-carotene-containing crystals, and calcium mineralizations.

2.2. Instrumentation

A schematic representation of the experimental setup is shown in Fig. 1. All Raman spectroscopic measurements were carried out using a confocal configuration in order to suppress signal contributions from the microenvironment of the selected morphologic structure. The studies were performed on a microscope (Zeiss Axioskop 50, Zeiss,

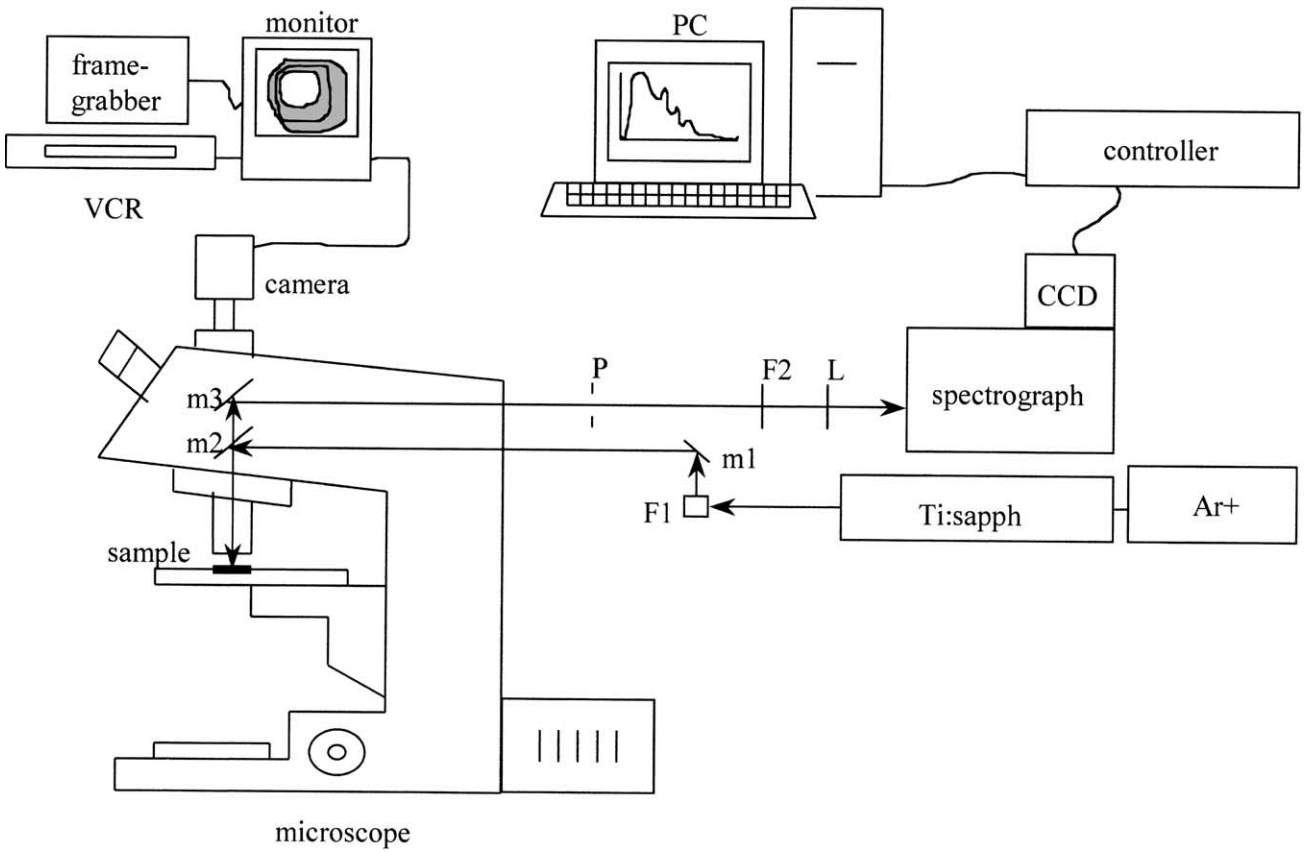

Fig. 1. A schematic representation of the confocal Raman microspectrometer. An 830-nm laser light is delivered by an Ar+ laser pumped Ti/sapphire laser system. The laser light is directed to the microscope through a holographic laser beampass filter (F1), a mirror (m1), and a dichroic beam splitter (m2). The light is focused onto a tissue sample through a high numerical aperture microscope objective. The scattered light is collected by the same objective, passes the beam splitter, and passes through a pinhole (P), which enables confocal detection. The remaining light is band pass filtered (F2) to remove remaining laser light, and is focused into the spectrometer using a lens (L). A removable mirror (m3) is used to direct either collected light from the sample to the spectrometer/CCD system, or white light images to the video camera system. Raman signals are collected by a personal computer and stored on the hard disk for later analysis. The video system is used to aim the laser light at the structures selected for investigation. Phase contrast images are stored on videotape (VCR) for later analysis.

Thornwood NY), fitted with a phase contrast system and a stage controller (1 μm step resolution; Prior Scientific Instruments, Cambridge, MA). Initial examination of the sample was performed with phase contrast microscopy at 10x magnification (Zeiss Achroplan objective). Detailed examination and microspectroscopy were performed with a 63 × infinitely corrected water immersion objective (Zeiss Achroplan, NA 0.9). The phase contrast tissue examination and morphologic structure selection for microspectroscopy were recorded using a CCD color video camera (Sony, Cambridge, MA) attached to the microscope and stored on video tape (VCR) from which frames were digitized (PCVision-plus, Imaging Technologies, Bedford, MA).

Near-infrared (830 nm) laser light was generated by An Ar+-pumped Ti/sapphire laser system (Coherent Innova 90/Spectra Physics 3900S, Coherent, Santa Clara, CA). The laser output was band pass filtered (F1) (Kaiser Optical Systems HLBF, Ann Arbor, MI) and focused onto the sample using an adjustable mirror (m1), and a dichroic beamsplitter (m2), with a laser power on the sample of 50–100 mW. Light emitted from the tissue sample was collected by the same objective, passed through the beamsplitter and passed through a pinhole (P: 100 μm diameter) by a removable mirror (m3). This mirror was used to direct either light emitted from the sample to the spectrometer/CCD system, or white light images to the video camera system. The remaining light was then Notch-filtered to reject Rayleigh scattered light (F2; Kaiser Optical Systems HSNF) and focused with an achromatic lens (L) into a Chromex 250IS/SM spectrograph-monochromator (Chromex, Albuquerque, NM). Inside the spectrograph, a grating dispersed light onto a deep-depletion CCD detector (Princeton Instruments, Princeton, NJ) cooled to −110°C. The CCD interface (ST130 Princeton Instruments) was connected to a personal computer using Winspec software (Princeton Instruments, version 1.4.3), which performed data processing and storage. At least three Raman spectra (sampling time between 10 and 100 s) over a range of 100–2000 cm^{-1} (8 cm^{-1} resolution) were obtained from each site selected (see also Section 2.4).

2.3. Performance of the confocal Raman microspectrometer

A previously described method was used to estimate the light collection or sampling volume of the confocal Raman microspectrometer [3]. A small ($1-2\ \mu m^3$) collection volume was needed to insure adequate resolution to collect Raman spectra from small or thin microscopic structures, such as individual collagen fibers. In short, polystyrene beads of 1.0-μm diameter (Polysciences, Warrington, PA) were moved through the focused laser beam, and the Raman signal was collected as a function of the bead position relative to the center of the laser focus. The step resolution of the microscope stage in the horizontal plane was 1 μm. Vertical displacement proceeded in 1.1-μm steps. The position was optimized to obtain the maximal Raman signal of the bead. Lateral resolution was determined by alternately measuring the Raman signal of the central position and one of eight positions in the *X* or *Y* direction from the center of the bead using 1- or 2-μm steps. The intensity of the strong 1004 cm^{-1} polystyrene Raman band was measured as a function of the distance to the laser focus in both the planar directions and the axial direction. The result for each direction was then fitted with a Gaussian function, and the diameter of the focused beam was determined from the full width at half-maximum intensity. For both lateral directions, the diameter was about 1 μm and for the axial direction was 2 μm. The sampling volume was calculated to be about 1 μm^3.

2.4. Data analysis

Data analysis of Raman spectra from morphologic structures was performed with Microcal Origin software (version 4.10, Clecom, Birmingham, UK). This analysis consisted of cosmic ray removal, wavenumber shift calibration using the spectral features of toluene (Mallinckrodt Specialty Chemicals, Paris, KY), and correction for chromatic variation in the filter/spectrometer/CCD detector system with a calibrated tungsten light source. The tissue spectra were then corrected for BaF_2 or MgF_2 background contribution by subtraction of the appropriate spectrum, and corrected for tissue fluorescence by subtraction of a fourth-order polynomial that was fitted to the spectrum by least-squares minimization (LSM) [30].

Each morphologic structure spectrum was modeled in the Raman shift range of 700–1800 cm^{-1}, using a simple linear combination model to generate fractional fit contributions (C_l) for each of the 12 biochemical components, *l*, as

$$r_{\text{total}} = C_1 r_1 + C_2 r_2 + C_3 r_3 \ \ldots$$

where *r* is the Raman spectrum. The 700–1800-cm^{-1} Raman shift range was chosen because this range contains most spectral information.

Reagent grade commercial chemicals were used to obtain the Raman spectra, for use as basis spectra, of the 12 biochemical components, including proteins (collagen type III, elastin, actin, myosin, and tropomyosin) (Sigma, St. Louis, MO), unesterified cholesterol (cholesterol monohydrate) (Sigma), cholesterol esters (cholesterol linoleate) (Sigma), phospholipids (phosphatidyl choline) (Sigma), triglycerides (triolein) (Sigma), carotenoids (β-carotene) (Sigma), and calcium salts (calcium hydroxyapatite and calcium carbonate) (Sigma). These 12 biochemical components were selected as the most common biochemical species found in normal arterial tissue and atherosclerotic plaque. Additionally, a similar set of biochemical constituents had provided good fit of the model to the observed spectrum in previous macroscopic tissue studies [21–31]. The Raman spectra from these chemicals were recorded in a similar way as the Raman spectra from the morphologic structures.

The model components could not be scaled on chemical weight, since the actual concentration of the biochemicals in the various morphologic structures is unknown. Therefore, as done in our previous studies, the intensity of the spectral feature at 1440–1455 cm^{-1} (representing CH_2 bonds in protein and lipid) was set to unity. The Raman spectra of β-carotene, calcium carbonate, and calcium hydroxyapatite, which lack spectral features in this region, were set to unity with respect to spectral features at 1159, 1080, and 961 cm^{-1}, respectively. This model thus provided information about the relative fit contribution of these chemical components to the Raman spectra of the various morphologic structures. The fit contribution of each biochemical component is expressed as a fraction of the maximum (i.e. 1).

3. Results

Fig. 2A is a photomicrograph of an unstained coronary artery section showing the internal elastic lamina viewed under phase contrast. This structure was examined at a total of 54 sites in 21 coronary artery samples. In nine of these samples, we also collected spectra from the external elastic lamina. In Fig. 2B, the Raman spectra of six different internal elastic laminae are shown. The bands at 1664 and 1264 cm^{-1} are attributable to the amide I and III vibrations, respectively, of structural proteins such as elastin and collagen [26,35,36]. The intense band at 1449 cm^{-1} can be assigned to the CH_2 and CH_3 bending mode of proteins [25,35], and the 1004 cm^{-1} band to phenylalanine [36]. The bands at 1336 and 1104 cm^{-1} are attributable to desmosine/isodesmosine [26], and are specific for elastin. The bands at 933 and 855 cm^{-1} can be assigned to the C–C stretching mode of proline [26,36] and are present in collagen. These results indicate that internal elastic lamina contains both elastin and collagen. Furthermore, on visual inspection, these spectra show very little variation from structure to structure, indicating that the biochemical composition of internal elastic lamina is very consistent within and between coronary artery samples. Spectra obtained from

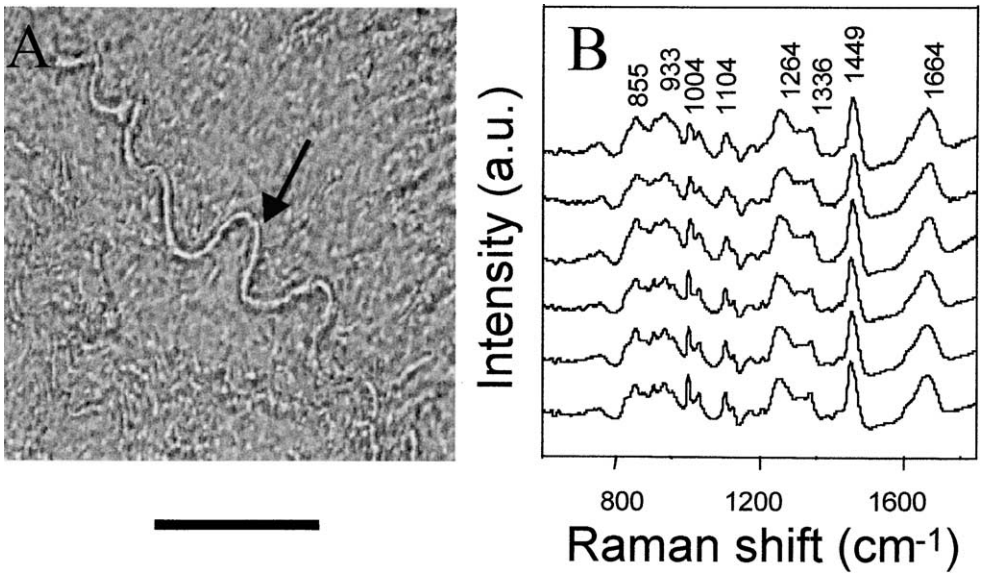

Fig. 2. (A) Photomicrograph of internal elastic lamina (arrow) in a 6-μm-thick unstained coronary artery section viewed under phase contrast. (B) The Raman spectrum of internal elastic laminae in six different coronary artery samples. Note that there are only slight variations between the spectra, indicating that the biochemical composition of internal elastic lamina is very consistent. Experimental conditions: laser power: 85 mW; collection time: 150 s. Scale bar: 40 μm.

the external elastic lamina (not shown) were identical to those obtained from the internal elastic lamina.

Fig. 3A is a phase contrast photomicrograph showing collagen fibers (length $\sim$10 μm, diameter $\sim$2 μm) in the connective tissue of the tunica adventitia. In total, 17 collagen fibers in 10 samples were studied. Fig. 3B shows the Raman spectra from collagen fibers from three different artery samples. Again, on visual inspection, these spectra collected from the adventitia (a, b) show little variation from fiber to fiber within or among coronary artery samples, and are identical to those taken from collagen fibers in the fibrous cap (c) of intimal atherosclerotic lesions. These spectra are also very similar to those from the elastic laminae, except for the absence of desmosine and isodesmosine bands (specific for elastin). The collagen fiber spectra also contain a pronounced hydroxyproline contribution (855 cm^{-1}) specific for collagen [26,36].

Fig. 4 shows four Raman spectra recorded from smooth muscle cells in the tunica media in normal and atherosclerotic coronary artery samples. In total, 32 spectra were recorded

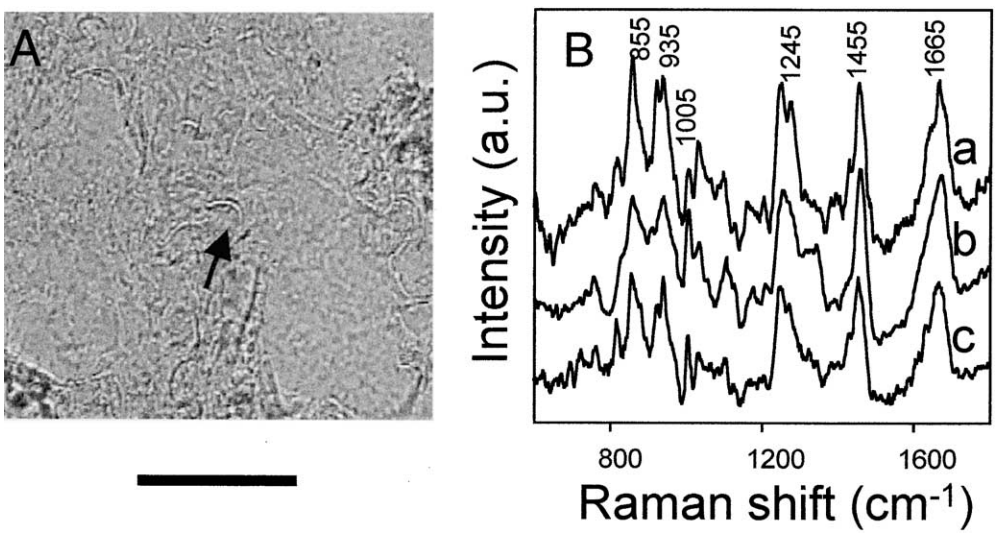

Fig. 3. (A) Photomicrograph of the tunica adventitia with collagen fibers in a 6-μm unstained coronary artery section viewed under phase contrast. (B) The Raman spectrum of collagen fibers in three different coronary artery samples: (a, b) adventitia, (c) fibrous cap. Experimental conditions: laser power: 80–105 mW; collection time: 180 s. Scale bar: 40 μm.

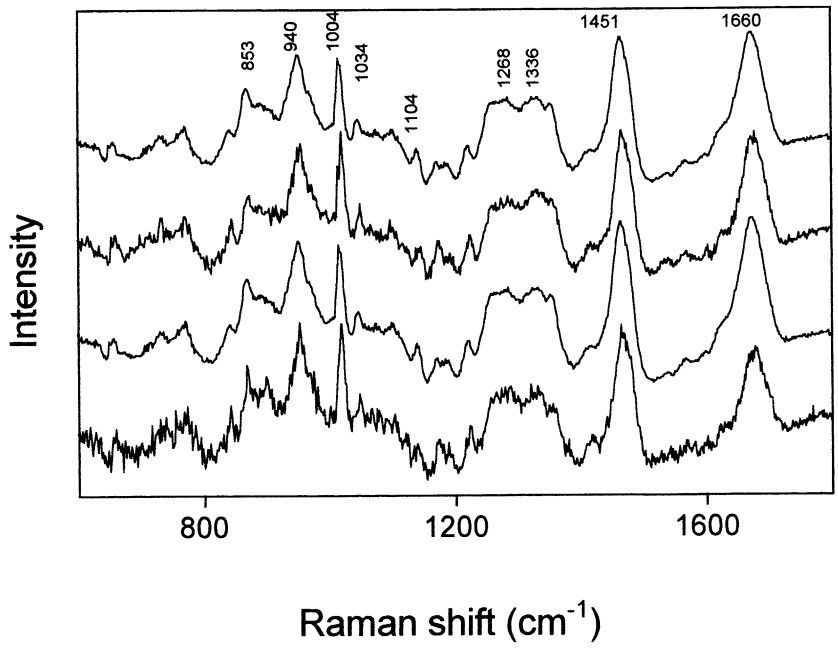

Fig. 4. The Raman spectra of four different smooth muscle cells in the tunica media. Experimental conditions: laser power: 75–100 mW; collection time: 120–180 s.

from 10 coronary artery samples. On visual inspection, no significant differences were observed between spectra taken from individual smooth muscle cells. The main spectral features in the smooth muscle cell spectra are similar to those observed in the elastic laminae and collagen fiber spectra, and are dominated by protein bands at 1660 and 1268 cm^{-1} (amide I and III vibrations, respectively) [35,37], 853, 940, 1034, 1336 and 1451 cm^{-1} (C–C or C–H bending) [35–37], and 1004 cm^{-1} (phenylalanine) [36]. The main differences between the protein-dominated smooth muscle cell, elastic laminae, and collagen fiber spectra are in intensity variations in the phenylalanine (1004 cm^{-1}) [36], desmosine/isodesmosine (1336 and 1104 cm^{-1}) [26] and amide III (1268 cm^{-1}) bands [35,37].

Fig. 5 shows examples of Raman spectra collected from fat cells (adipocytes) in the tunica adventitia. In total, eight

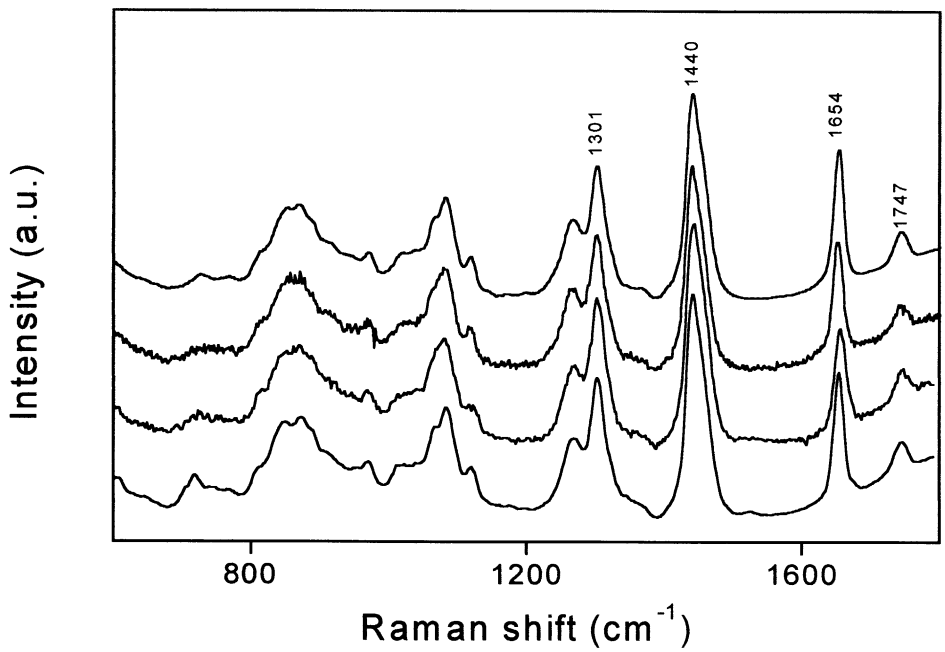

Fig. 5. The Raman spectra of four fat cells (adipocytes) in the tunica adventitia. Experimental conditions: laser power: 70–85 mW; collection time: 60–120 s.

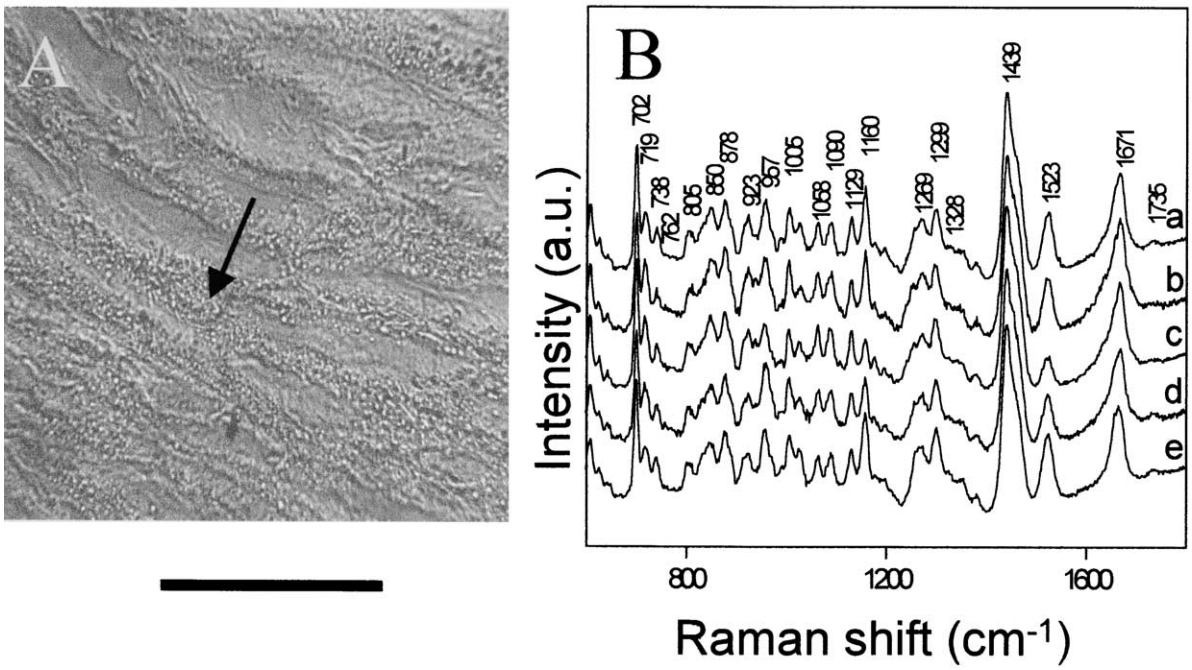

Fig. 6. (A) Photomicrograph of foam cells in an intimal atherosclerotic plaque in a 6-μm unstained coronary artery section viewed under phase contrast. (B) Raman spectra of foam cells (a–c) and necrotic core (d and e). Experimental conditions: laser power: 65 mW; collection time: 120 s. Scale bar: 40 μm.

adipocytes were examined from six coronary artery samples. The spectra collected from the fat cells were very similar, and are dominated by an ester band (1747 cm^{-1}), an unsaturated carbon/carbon band (C=C; 1654 cm^{-1}), and CH_2/CH_3bands (1440 and 1301 cm^{-1}), which, in combination, indicate triglycerides [23,25].

Fig. 6A is a phase contrast photomicrograph of foam cells in the intima of an atheromatous plaque. The individual lipid droplets in these cells can easily be identified. In total, 30 foam cells in eight coronary artery samples were studied. In Fig. 6B, the Raman spectra from three foam cells are shown (a–c). Although similar on visual inspection, these spectra show more variation among foam cells than the spectra of collagen fibers, the internal and external elastic laminae, and smooth muscle cells (see Figs. 2B, 3, and 4). More specifically, the foam cell spectra are distinctly different from the

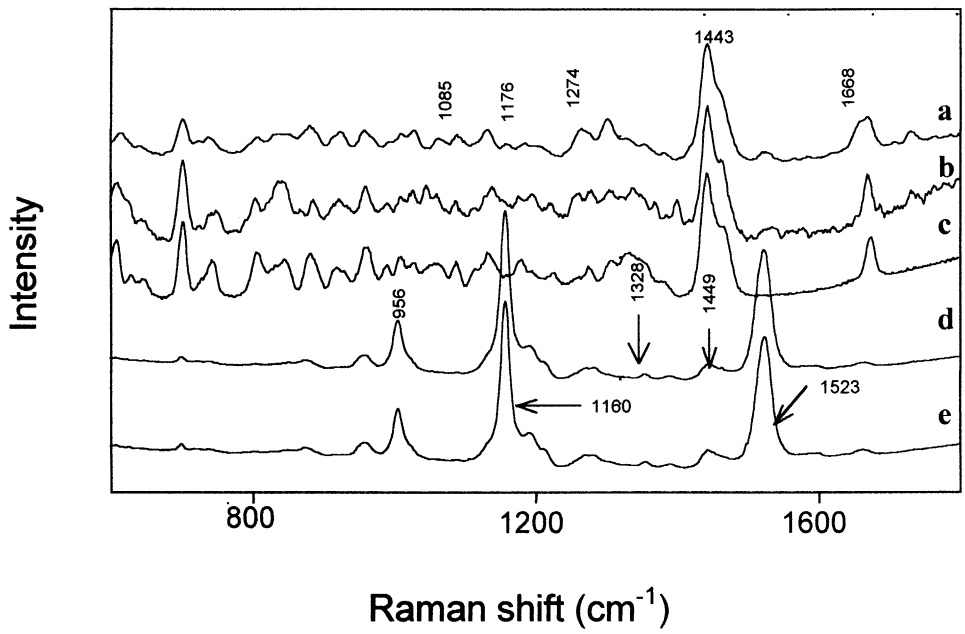

Fig. 7. The Raman spectra of cholesterol crystals (a–c) and yellow colored crystals (d and e) in intimal atherosclerotic plaques.

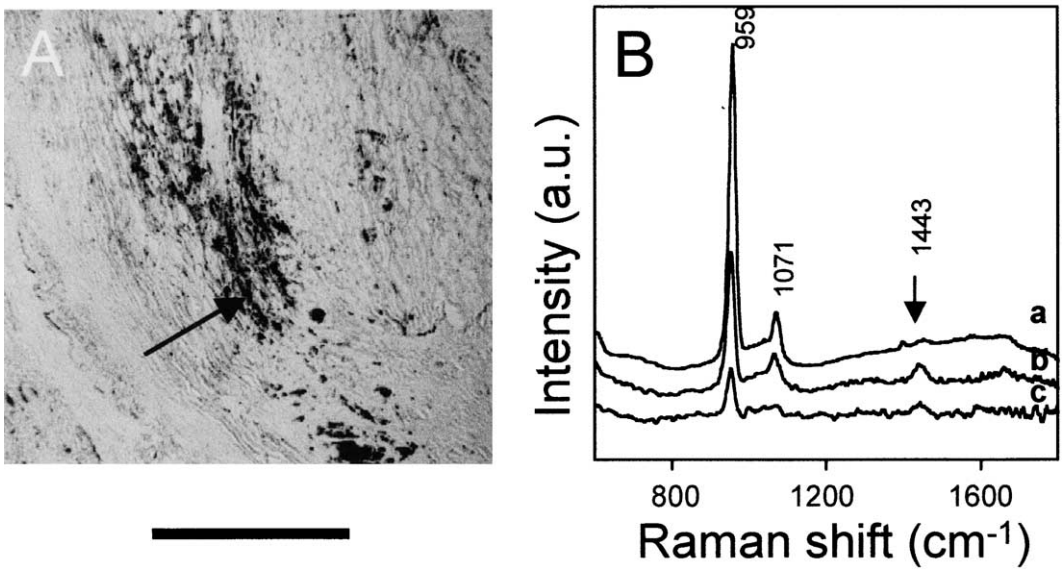

Fig. 8. (A) Photomicrograph of the a calcification in the necrotic core of an intimal atherosclerotic plaque (arrow) in a 6-μm unstained coronary artery section viewed under phase contrast. (B) Raman spectra of three calcified plaques in various stages of calcification. These spectra are scaled with respect to the 1444 cm^{-1} band. Also present in the spectra of less calcified plaques with punctate calcium mineralizations spectra are steroid nucleus features (around 700 cm^{-1}) indicative of cholesterol. Experimental conditions: laser power: 75 mW; collection time: 60 s. Scale bar: 200 μm.

protein-dominated spectra of the elastic laminae, collagen fibers, and smooth muscle cells, particularly with regard to the numerous bands below 1100 cm^{-1}. The bands at 702, 878, 923, and 957 cm^{-1} can be assigned to the steroid nucleus of both unesterified (free) cholesterol and cholesterol esters [25]. The intense bands at 1671, 1439, 1299, and 1270 cm^{-1} are due to C=C stretch and CH_2/CH_3 bending modes [23,25,35]. The presence of bands at 1735 and 1026 cm^{-1}

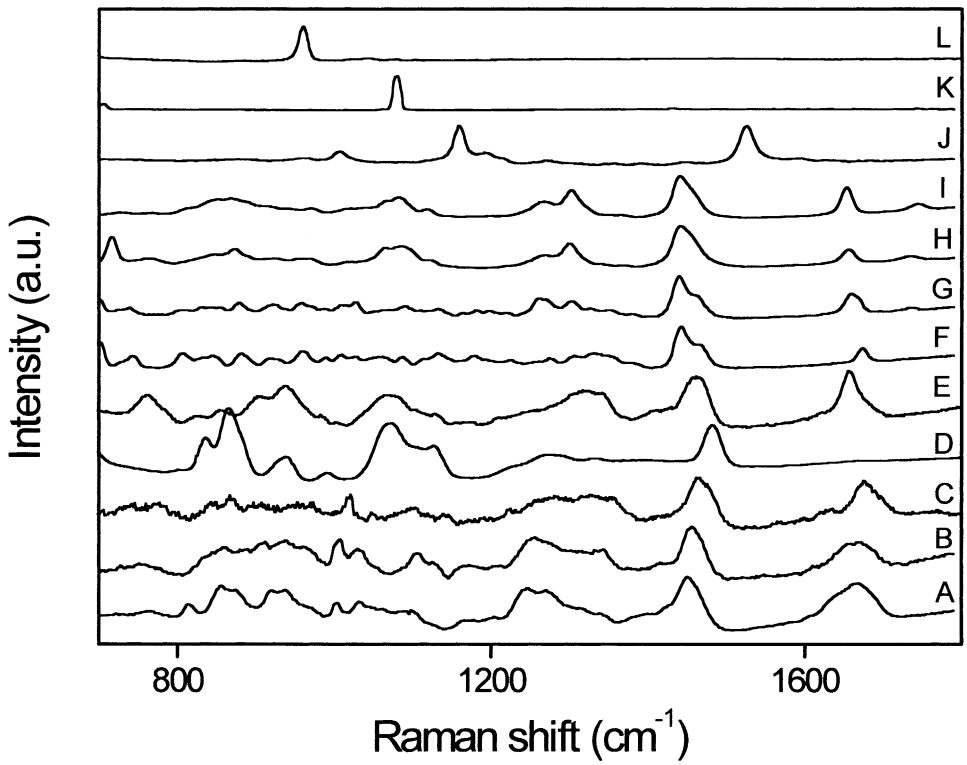

Fig. 9. Raman basis spectra of the 12 biochemicals used for linear fitting to the morphologic spectra. (A) Collagen (type III), (B) elastin, (C) actin, (D) myosin, (E) tropomyosin, (F) cholesterol monohydrate, (G) cholesterol linoleate, (H) phosphatidyl choline, (I) triolein, (J) β-carotene, (K) calcium carbonate, and (L) calcium hydroxyapatite.

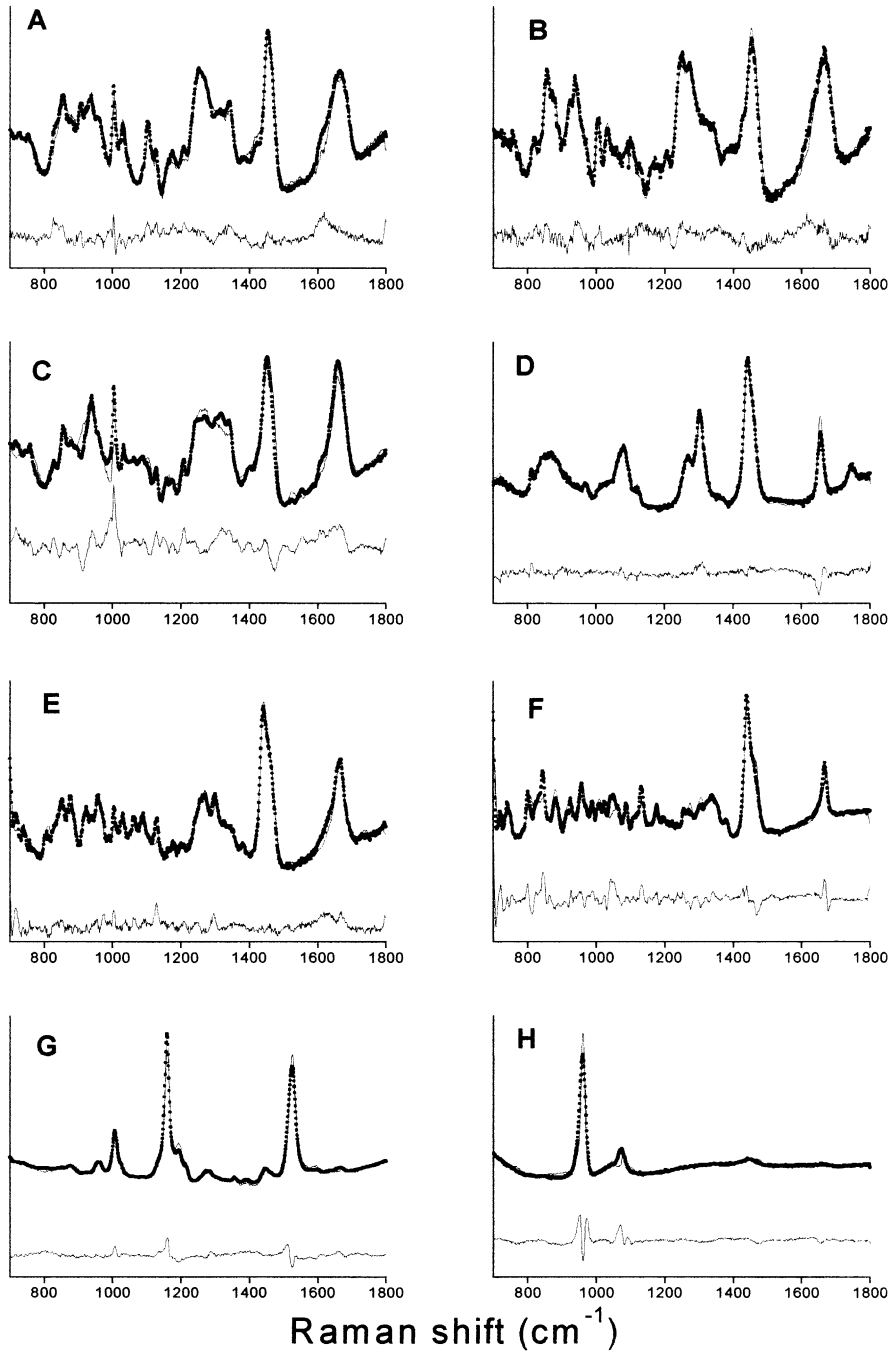

Fig. 10. Comparison between data (dots) and model fit (line) of spectra of the morphologic structures in coronary artery. (A) Internal/external elastic lamina, (B) collagen fiber (C) smooth muscle cell, (D) fat cell, (E) foam cell/necrotic core, (F) cholesterol crystal, (G) β crystal, and (H) calcification.

(specific for cholesterol esters) [25] and 1058 and 1328 cm^{-1} (specific for free cholesterol) [23,25,38] indicates that these foam cells contain both esterified and unesterified cholesterol. The bands at 719 cm^{-1} (symmetric choline stretch), 762 cm^{-1} (symmetric O–P–O stretch), and 878 cm^{-1} (asymmetric O–P–O stretch) indicate the presence of phospholipids [38], and those at 1523 and 1160 cm^{-1} the presence of β-carotenoids [26,39]. However, the foam cell spectra lack the triglyceride bands at 1747, 1654, 1440, and 1301 cm^{-1} seen in adventitial fat cells.

In total, 31 necrotic core regions in 16 coronary artery samples were studied. Fig. 6B also shows two examples of Raman spectra collected from necrotic core (d and e). Similar to the foam cell spectra, there is some variation from structure to structure within the necrotic core. However, the average spectra from foam cells and necrotic core are quite similar, indicating that the chemical contents of both morphologic structures are quite similar.

Fig. 7(a–c) shows examples of Raman spectra taken from cholesterol crystals of different size in the necrotic core of

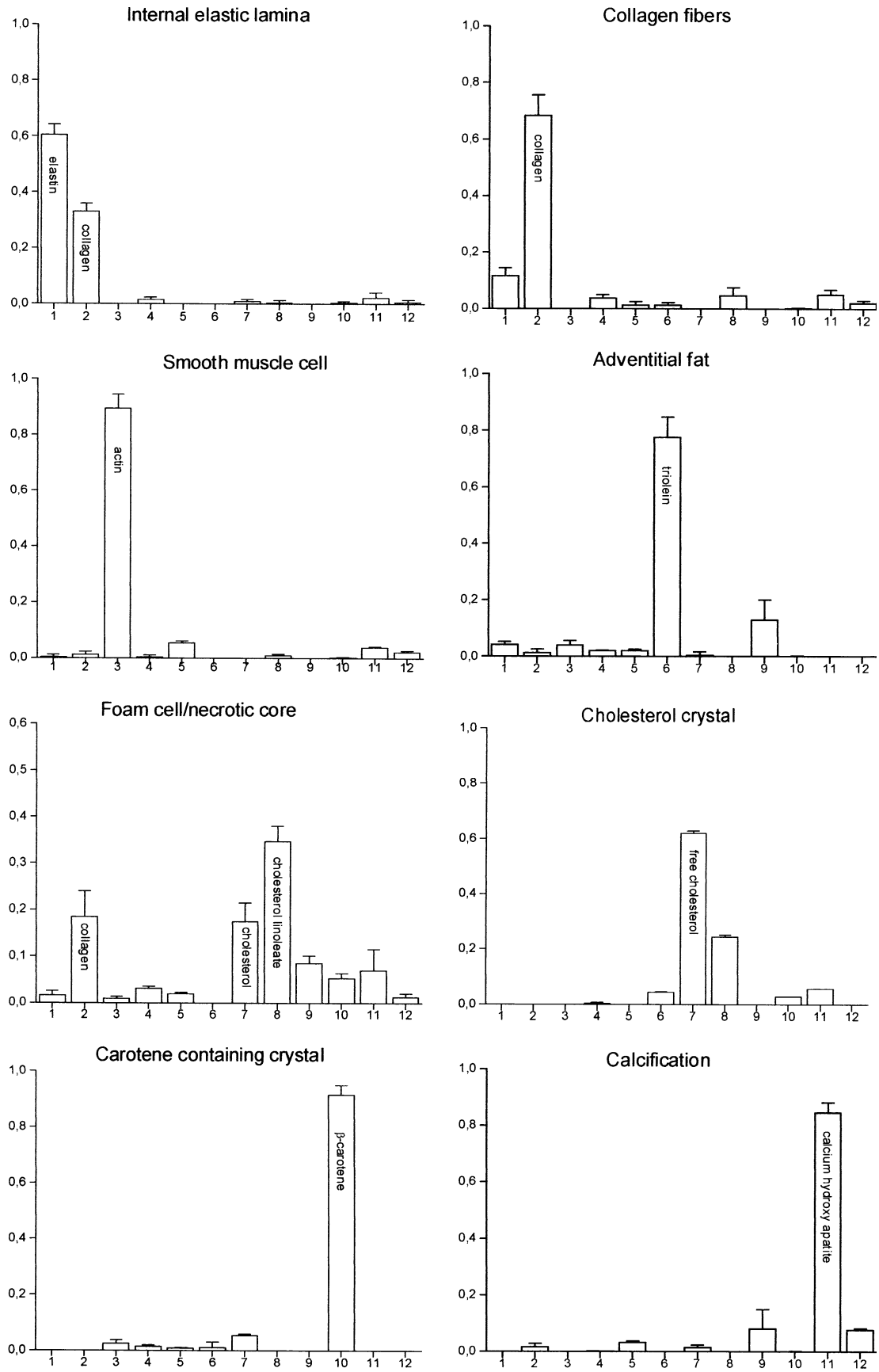
Internal elastic lamina
elastin
collagen
Collagen fibers
collagen
Smooth muscle cell
actin
Adventitial fat
triolein
Foam cell/necrotic core
collagen
cholesterol
cholesterol linoleate
Cholesterol crystal
free cholesterol
Carotene containing crystal
β-carotene
Calcification
calcium hydroxy apatite

atheromatous plaques. In total, 10 cholesterol crystals in seven coronary artery samples were studied. The main spectral features of the cholesterol crystal spectra are at 1668 cm^{-1} (C=C stretch), 1443, 1328, and 1274 cm^{-1} (CH_2, CH_3bending), and 1176 and 1085 cm^{-1} (C−C stretch) [23,25,35]. The spectral features below 1000 cm^{-1} are attributed to steroids, indicating the presence of unesterified cholesterol. Slightly more variation was seen between the spectra from individual crystals, mainly due to band intensity variations, indicative of differences in the ratio of free to esterified cholesterol in the crystals themselves or in the tissue components surrounding the crystals.

In necrotic core regions, yellow crystals could be identified under phase contrast occasionally. Fig. 7(d and e) shows the Raman spectra of two such crystals from two different coronary artery samples. In total, seven of these crystals from three samples were studied. The main spectral features are bands at 1523 and 1160 cm^{-1}, which are due to C−C and C=C stretches and indicative of β-carotene [26,39]. Given the presence of bands at 1449 and 956 cm^{-1}, these yellow crystals also appear to contain some structural proteins and cholesterol esters.

Fig. 8A is a photomicrograph of an atherosclerotic plaque containing a calcification. In total, 15 calcium mineralizations in six coronary artery samples were studied. Raman spectra representing different stages of calcification in two atherosclerotic plaques are shown in Fig. 8B. The main features of these spectra are 1071 and 959 cm^{-1} bands attributed to CO_3^{2-} (symmetric)/PO_4^{3-} (asymmetric) and PO_4^{3-} (symmetric) stretches, indicative of calcium carbonate and calcium hydroxyapatite, respectively [40,41]. Large calcium mineralizations (Fig. 8B, a and b) show spectral features different from those of minute punctate calcium mineralizations in the necrotic core (Fig. 8B, c). The main difference is the presence of additional features in the spectra of the punctate calcium mineralizations attributable to lipids and/or phospholipids (1443 cm^{-1}), most likely due to the surrounding necrotic core.

3.1. Biochemical modeling results

Using the basis spectra of pure chemicals (Fig. 9), the spectra of the individual morphologic structures were fitted in the biochemical model. Each panel in Fig. 10 shows a Raman spectrum of one of the morphologic structures, and the result of the least-squares minimization fit of the biochemical model. Residuals (data minus the fit) are shown on the same scale. Because the Raman spectra from foam cells and necrotic core were very similar, only the fit results of the foam cells are shown. Judging from the residuals of the fits to the observed spectra, which are on the order of magnitude of the noise and show no consistent pattern from spectrum to spectrum, the Raman spectrum of each morphologic structure (panels A–H) is well described using the 12 biochemical basis spectra.

For each morphologic structure examined, the contribution of each biochemical component was determined. Fig. 11 confirms that each morphologic structure has a characteristic biochemical composition. Generally, each morphologic structure is composed largely of one or two major biochemical components, combined with one or more less abundant biochemical components.

The internal and external elastic laminae (Fig. 11A) are mainly composed of elastin with a smaller collagen component, whereas collagen fibers in both normal arteries and the fibrous cap of atherosclerotic lesions (Fig. 11B) are mainly composed of collagen with a small elastin component. Smooth muscle cells (Fig. 11C) were modeled almost entirely by actin and a small tropomyosin component. Myosin did not contribute at all.

Adventitial fat cells (Fig. 11D) contain almost exclusively triglycerides (triolein) with a small contribution of phospholipids (phosphatidyl choline). In contrast, foam cells and necrotic core (Fig. 11E) contain mainly cholesterol esters (linoleate) and free cholesterol (monohydrate) at a ratio of about 2:1, with smaller contributions of collagen, phospholipids, and β-carotene. Foam cells could not be distinguished from necrotic core on the basis of their biochemical composition. Cholesterol crystals (Fig. 11F) contain free cholesterol and cholesterol ester at a ratio of about 3:1. The yellow crystals (Fig. 11G) consist almost entirely of β-carotene, with a small contribution of cholesterol. This may indicate that these crystals are in fact cholesterol crystals that contain high concentrations of β-carotene. Calcium mineralizations (Fig. 11H) are mainly composed of calcium hydroxyapatite with small contributions of collagen, triglycerides, and calcium carbonate.

4. Discussion

Current atherosclerosis research focuses on unstable plaques, with a thin fibrous cap overlying a large pool of necrotic lipid material (the atheroma) comprised largely of cholesterol [10–12]. Recent studies have shown that chemical composition and morphology, rather than anatomy (degree of stenosis), determine atherosclerotic plaque stability and predict disease progression and the risk of life-threatening complications such as thrombosis and acute plaque hemorrhage [13–21]. For example, the presence of cholesterol

Fig. 11. The biochemical fit contributions to the spectra of: internal/external elastic laminae, collagen fibers, smooth muscle cell, adventitial fat, foam cells/necrotic core, cholesterol crystal, β crystal, and calcification. The biochemicals are: (1) elastin, (2) collagen (type III), (3) actin, (4) myosin, (5) tropomyosin, (6) triolein, (7) cholesterol monohydrate, (8) cholesterol linoleate, (9) phosphatidyl choline, (10) β-carotene, (11) calcium hydroxyapatite, and (12) calcium carbonate. Data are presented as means ± S.D.

esters may soften the plaque, whereas crystalline-free cholesterol may have the opposite effect [18,19]. The presence of foam cells and other inflammatory cells may also play a role in plaque instability [20,21]. Therefore, morphologic factors, such as the presence of crystalline-free cholesterol or foam cells, may be as important as biochemical composition in determining atherosclerotic plaque stability and progression.

A diagnostic technique that can analyze plaque morphology in vivo might prove extremely useful in the clinical evaluation of atherosclerotic lesions. This study investigates the feasibility of morphologic analysis of atherosclerotic lesions in coronary arteries using Raman spectroscopy, a technique that can analyze tissue components in situ in their microenvironment within intact (nonhomogenized, nonextracted) tissues, and can potentially be performed in vivo using optical fiber technology.

To that end, we determined the spectral signatures of the cellular and extracellular morphologic components of normal and atherosclerotic arterial tissue in situ using confocal Raman microspectroscopy. The specific morphologic structures were selected because of their role in normal arterial anatomy (e.g. elastic laminae) and/or atherosclerotic plaque formation (e.g. foam cells, necrotic core, cholesterol crystals) [42]. Least-squares minimization of a linear combination of the basis spectra of 12 biochemical components provided information on the biochemical composition of the various morphologic structures. These biochemical components were selected because they were known to be present in high concentration in normal arterial tissue and/or atherosclerotic plaque (e.g. collagen, elastin, and free and esterified cholesterol) [35–41] or because they are strong Raman scatterers (e.g. β-carotene) [42–51]. Glycosaminoglycans (e.g. hyaluronic acid, chondroitin sulfate, dermatan sulfate, and heparan sulfate), which may contribute 3% of artery dry mass [45,49], did not contribute significantly to the biochemical model fits, most likely because they are weak Raman scatterers (i.e. they have small Raman cross sections). They were therefore excluded from the model.

As was shown in Fig. 9, the biochemical model described the spectrum of each morphologic structure quite well, which means that the most essential biochemical components were included in the model. The biochemical composition of each structure, indicated by the fit contributions of the biochemical basis spectra to the morphologic structure spectrum, was very consistent (Fig. 10). The largest biochemical variations were found in foam cells, necrotic core, cholesterol crystals, and calcium mineralizations. The biochemical variations in both calcium mineralizations, cholesterol crystals, and β-carotene-containing crystals may be due to differences in their stage of progression (as reflected by size) [53,54]. The cause of the biochemical variations within foam cells and necrotic core (differences in collagen, β-carotene, and cholesterol esters) is less clear. Variations in the lipid composition of atherosclerotic plaques at various stages of progression have been described previously in in vitro studies of homogenized or extracted tissues and cultured monocyte-derived foam cells [45–47,50,55,56]. However, the biochemical data reported in the present study are the results of analysis of atherosclerotic plaque components in situ, without the confounding effects of tissue preparation or in vitro cell culture models. More detailed in situ Raman microspectroscopy studies of foam cells and necrotic cores in atherosclerotic plaques at various stages of disease progression may help to further elucidate the origin of this variation.

Although the biochemical model did provide valuable information on the biochemical composition of the microscopic cellular and extracellular morphologic structures, it has its limitations. One of the major limitations of this model was illustrated by the fits of the smooth muscle cell spectra. Previous in vitro studies [57] have shown that smooth muscle cells, which comprise the majority of the tunica media of muscular arteries such as the coronary artery, contain approximately three times more actin than myosin, but approximately equal amounts of myosin and tropomyosin [52]. However, the fit contributions in the biochemical model indicated that smooth muscle cells contained almost exclusively actin, with a small amount of tropomyosin and virtually no myosin. These unexpected results may be due to conformational differences in spectroscopic characteristics of myosin between tissue-extracted myosin and intracellular myosin in situ. In addition, as seen with the glycosaminoglycans, the contribution of weak Raman scatterers may be underestimated.

Observed variations may also be due to contributions of biochemical compounds that are not included in the model. For example, only one class of collagen was included. This should not be a great concern, as we have seen little difference in the Raman spectrum of the different classes of collagens in vitro [unpublished results]. However, there may be significant changes in the Raman spectra of collagen in vivo due to increased crosslinking as atherosclerotic lesions progress. Further studies with additional model components may improve its performance in this respect. However, the degree of improvement of the model is expected to be limited by technical considerations, such as wavenumber calibration and S/N.

Despite these limitations, the results of our previous quantitative Raman spectroscopy biochemical analyses of normal and atherosclerotic arterial tissue, using the same biochemical model, compared well with standard analytical techniques [24–29]. Previous studies have also shown that these quantitative Raman spectroscopy biochemical analyses could be used as the basis of a diagnostic algorithm that accurately classified arterial tissues as either nonatherosclerotic or calcified or noncalcified atherosclerotic plaque [31]. The results of the present study show that a modification of the biochemical model can be used to perform a relative comparison of cellular and extracellular morphologic components of normal and atherosclerotic arterial tissue. Furthermore, a follow-up study shows that these relative

morphologic comparisons can be used as the basis for an algorithm that allows diagnosis of atherosclerosis in coronary arteries [32]. This is the first step in developing a quantitative Raman spectroscopy morphologic analysis with the purpose to accurately classify normal arteries and atherosclerotic plaques ex vivo, and in the future to predict plaque stability and disease progression in vivo [33].

5. Conclusion

Using our biochemical model, we have shown for the first time that confocal Raman microspectroscopy can be used to perform an in situ biochemical analysis of individual microscopic morphologic structures (such as foam cells and necrotic core) in intact arterial tissues that cannot be isolated or purified using conventional analytical techniques. Furthermore, we have shown that the various morphologic structures have characteristic Raman spectra, which, as expected, vary little from structure to structure or from artery to artery, and can be used as basis spectra in a morphologic model to perform a relative comparison of the morphology of normal and atherosclerotic coronary arteries ex vivo. This nondestructive technique may ultimately be used to assess plaque stability and disease progression in humans in vivo, as well as to study atherogenesis in animal models and lipid metabolism in cell cultures in vitro.

Acknowledgments

Financial support from the Interuniversity Cardiology Institute of the Netherlands (ICIN D96.2158/MH) and the NIH (grant: P41RR02594) is gratefully acknowledged. The authors wish to thank Dr. Ramasamy Manoharan for stimulating discussions. The research was conducted at the MIT Laser Biomedical Research Center, Cambridge, MA, USA.

References

[1] Hawi SR, Nithipathikom K, Wohlfeil ER, Adar F, Campbell WB. Raman microspectroscopy of intracellular cholesterol crystals in cultured bovine coronary artery endothelial cells. J Lipid Res 1997; 38:1591–7.

[2] Puppels GJ, de Mul FFM, Otto C, Greve J, Robert-Nicoud M, Arndt-Jovin DJ, Jovin TM. Studying single living cells and chromosomes by confocal Raman microspectroscopy. Nature 1990;347:301–3.

[3] Puppels GJ, Colier W, Olminkhof JHF, Otto C, de Mul FFM, Greve J. Description and performance of a highly sensitive confocal Raman microspectrometer. J Raman Spectrosc 1991;22:217–25.

[4] Mizumo A, Ozaki Y, Kamada Y, Miyazaki H, Itoh K, Iriyama K. Direct measurement of Raman spectra of intact lens in a whole eyeball. Curr Eye Res 1981;1:609–13.

[5] Bakker Schut TC, Puppels GJ, Kraan YM, Greve J, van der Maas LLJ, Figdor CG. Intracellular carotenoid levels measured by Raman microspectroscopy: comparison of lymphocytes from lung cancer patients and healthy individuals. Int J Cancer 1997;74:20–5.

[6] Gniadecka M, Wulf HC, Nielsen OF, Christensen DH, Hercogova J. Distinctive molecular abnormalities in benign and malignant skin lesions: studies by Raman spectroscopy. Photochem Photobiol 1997; 66:418–23.

[7] Hawi SR, Campbell WB, Kajdacsy-Balla A, Murphy R, Adar F, Nithipatikom K. Characterization of normal and malignant hepatocytes by Raman microspectroscopy. Cancer Lett 1996;110:35–40.

[8] Benedetti E, Teodori L, Trinca ML, Vergamini P, Salvati F, Spremolla G. A new approach to the study of human solid tumor cells by means of FT-IR microspectroscopy. Appl Spectrosc 1990;44:1276–80.

[9] Wong PTT, Rigas B. Infrared spectra of microtome sections of human colon tissues. Appl Spectrosc 1990;44:1715–8.

[10] Richardson PD, Davies MJ, Born GV. Influence of plaque configuration and stress distribution on fissuring of coronary atherosclerotic plaques. Lancet 1989;2:941–4.

[11] Fuster V, Badimon L, Badimon J, Chesebro J-T. The pathogenesis of coronary artery disease and the acute syndromes. N Engl J Med 1992; 326:242–250, 310–318 (two articles).

[12] Woolf N, Davies MJ. Arterial plaque and thrombus formation. Sci Am Sci Med 1994;9:38–47.

[13] Loree HM, Tobias BJ, Gibson LJ, Kamm RD, Small DM, Lee RT. Mechanical properties of model atherosclerotic lesion lipid pools. Arterioscler Thromb 1994;14:230–4.

[14] Libby P. Molecular bases of the acute coronary syndromes. Circulation 1995;91:2844–50.

[15] Fishbein MC, Siegal RJ. How big are coronary atherosclerotic plaques that rupture? Circulation 1996;94:2662–6.

[16] Mann JM, Davies MJ. Vulnerable plaque: relation of characteristics to degree of stenosis in human coronary arteries. Circulation 1996; 94:928–31.

[17] Wexler L, Brundage B, Crouse J, Detrano R, Fuster V, Maddahi J, Rumberger J, Stanford W, White R, Taubert K. Coronary artery calcification: pathophysiology, epidemiology, imaging methods, and clinical implications: a statement for health professionals from the American Heart Association. Circulation 1996;94:1175–92.

[18] Libby P, Schoenbeck U, Mach F, Selwyn AP, Ganz P. Current concepts in cardiovascular pathology: the role of LDL cholesterol in plaque rupture and stabilization. Am J Med 1998;104:14S–8S.

[19] Kullo IJ, Edwards WD, Schwartz RS. Vulnerable plaque: pathobiology and clinical implications. Ann Intern Med 1998;129:1050–60.

[20] Matsuda Y, Kramer JR, Matsuda M. Progression and regression of coronary artery disease-linkage of clinical, pathologic, and angiographic findings. Clin Cardiol 1995;18:412–7.

[21] Burke AP, Farb A, Malcolm GT, Liang Y-H, Smialwk JE, Virmani R. Plaque rupture and sudden death related to exertion in men with coronary artery disease. JAMA, J Am Med Assoc 1999;281:921–6.

[22] Baraga JJ, Feld MS, Rava RP. In situ optical histochemistry of human artery using near-infrared Fourier transform Raman spectroscopy. Proc Nat Acad Sci U S A 1992;89:3473–7.

[23] Baraga JJ, Feld MS, Rava RP. Rapid near-infrared Raman spectroscopy of human tissue with a spectrograph and CCD detector. Appl Spectrosc 1992;46:187–90.

[24] Brennan JF. Near infrared Raman spectroscopy for human artery histochemistry and histopathology. PhD dissertation. Cambridge, MA: Massachusetts Institute of Technology, 1995.

[25] Manoharan R, Baraga JJ, Feld MS, Rava RP. Quantitative histochemical analysis of human artery using Raman spectroscopy. J Photochem Photobiol 1992;16:211–33.

[26] Manoharan R, Wang Y, Feld MS. Histochemical analysis of biological tissues using Raman spectroscopy. Spectrochim Acta Mol Spectrosc 1996;52:215–49.

[27] Salenius JP, Brennan JF, Miller A, Wang Y, Aretz T, Sacks B, Dasari MS, Feld MS. Biochemical composition of human peripheral arteries examined with near-infrared Raman spectroscopy. J Vasc Surg 1998; 27:710–9.

[28] Römer, TJ. Raman spectroscopy of arterial wall: an optical technique for quantitative chemical analysis of atherosclerotic lesions in situ. PhD dissertation, Leiden University, The Netherlands, 1999.
[29] Brennan JF, Römer TJ, Lees RS, Tercyak AM, Kramer JR, Feld MS. Determination of human coronary artery composition by Raman spectroscopy. Circulation 1997;96:99–105.
[30] Brennan JFB, Wang Y, Dasari RR, Feld MS. Near-infrared Raman spectrometer systems for human tissue studies. Appl Spectrosc 1997; 51:201–8.
[31] Römer TJ, Brennan JF, Fitzmaurice M, Feldstein ML, Deinum G, Myles JL, Kramer JR, Lees RS, Feld MS. Histopathology of human coronary atherosclerosis by quantifying its chemical composition with Raman spectroscopy. Circulation 1998;97:878–85.
[32] Buschman HP, Motz JT, Deinum G, Römer TJ, Fitzmaurice M, Kramer JR, van der Laarse A, Bruschke AV, Feld MS. Diagnosis of human coronary atherosclerosis by morphology-based Raman spectroscopy. Cardiovasc Pathol 2001;10:59–68.
[33] Buschman HP, Marple ET, Wach ML, Bennett B, Bakker Schut TC, Bruining HA, Bruschke AV, van der Laarse A, Puppels GJ. In vivo determination of the molecular composition of artery wall by Raman spectroscopy. Anal Chem 2000;72:3771–5.
[34] Shim MG, Song LM, Marcon NE, Wilson BC. In vivo near-infrared Raman spectroscopy: determination of feasibility during clinical gastrointestinal endoscopy. Photochem Photobiol 2000;72:146–50.
[35] Diem M. Introduction to modern vibrational spectroscopy. New York: Wiley 1993.
[36] Sadtler Standard Spectra. Philadelphia (PA): Sadtler Research Laboratories, 1974.
[37] Carey PR. Biochemical applications of Raman and resonance Raman spectroscopy. New York: Acad Press 1982.
[38] Sufra S, Dellepiane G, Masetti G, Zerbi G. J Raman Spectrosc 1977;6:267–71.
[39] Barnes MJ. Collagens in atherosclerosis. Coll Relat Res 1985;5:65–97.
[40] Faiman R. Raman spectroscopic studies of different forms of cholesterol and its derivatives in the crystalline state. Chem Phys Lipids 1977;18:84–104.
[41] Nelson DGA, Williamson BE. Raman spectra of phosphate and monofluorphosphate ions ion several dentally-relevant materials. Caries Res 1985;19:113–21.
[42] Rubin E, Farber JL. Pathology. Philadelphia, (PA): Lippincott 1994.
[43] Steinberg D, Witztum JL. Lipoproteins and atherogenesis. Current concepts. JAMA, J Am Med Assoc 1990;264:3047–52.
[44] Blankenhorn DH. The infiltration of carotenoids into human atheromas and xanthomas. Ann Intern Med 1960;53:944–54.
[45] Smith EB. Acid glucosaminoglycan, collagen and elastin content of normal artery, fatty streaks and plaques. Adv Exp Med Biol 1974; 43:125–39.
[46] Katz SS, Small DM, Smith FR, Dell RB, Goodman DS. Cholesterol turnover in lipid phases of human atherosclerotic plaque. J Lipid Res 1982;23:733–7.
[47] Lundberg B. Chemical composition and physical state of lipid deposits in atherosclerosis. Atherosclerosis 1985;56:93–110.
[48] Rokosova B, Rapp JH, Porter JM, Bentley JP. Composition and metabolism of symptomatic distal aortic plaque. J Vasc Surg 1986;3:617–22.
[49] Small DM. Progression and regression of atherosclerotic lesions: insight from lipid physical biochemistry. Arteriosclerosis 1988;8: 103–29.
[50] Guyton JR, Klemp KF. Development of the atherosclerotic core region. Arterioscler Thromb Vasc Biol 1994;14:1305–14.
[51] Felton CV, Crook D, Davies MJ, Oliver MF. Relation of plaque lipid composition and morphology to the stability of human aortic plaques. Arterioscler Thromb Vasc Biol 1997;17:1337–45.
[52] Caillé J-P, Pigeon-Gosselin M, Pézolet M. Laser Raman study of internally perfused muscle fibers; effect of Mg2+, ATP and Ca2+. Biochim Biophys Acta 1983;758:121–7.
[53] Hirsch D, Azoury R, Sarig S, Kruth HS. Colocalization of cholesterol and hydroxyapatite in human atherosclerotic lesions. Calcif Tissue Int 1993;52:94–8.
[54] Sarig S, Utian WH, Sheean LA, Gorodeski GI. Distribution of unesterified cholesterol-containing particles in human atherosclerotic lesions. Am J Pathol 1995;146:139–47.
[55] Garner B, Baoutina A, Dean RT, Jessup W. Regulation of serum-induced lipid loaded macrophages in atherosclerotic tissue has led to the development of in vitro systems to elucidate the mechanisms involved in lipid accumulation. Atherosclerosis 1997;128:47–58.
[56] Tabas I. Phospholipid metabolism in cholesterol-loaded macrophages. Curr Opin Lipidol 1997;8:263–7.
[57] Hartshorne DJ, Gorecka A. Biochemistry of the contractile proteins of smooth muscle. In: Bohr DF, Somlyo AP, Sparns HV, editors. Handbook of Physiology: the cardiovascular system II. Bethesda, (MD): The American Physiological Society 1980. p. 93–120.